Electronic Supplementary Information

Dopamine-modified cobalt spinel nanoparticles as active catalysts for acidic oxygen evolution reaction

Zhengle Chen[a], Zhiqing Yang[a], Xinyuan Li[a], Longhua Li[a,*] and Hua Lin[b,*]

[a]*School of Chemistry and Chemical Engineering, Jiangsu University, Zhenjiang 212013, P. R. China*

[b]*State Key Laboratory of Structural Chemistry, Fujian Institute of Research on the Structure of Matter, Chinese Academy of Sciences, Fuzhou 350002, P. R. China*

Table S3 Bader charges (*e*) of carbonaceous component (CC) and the Co_3O_4 component.

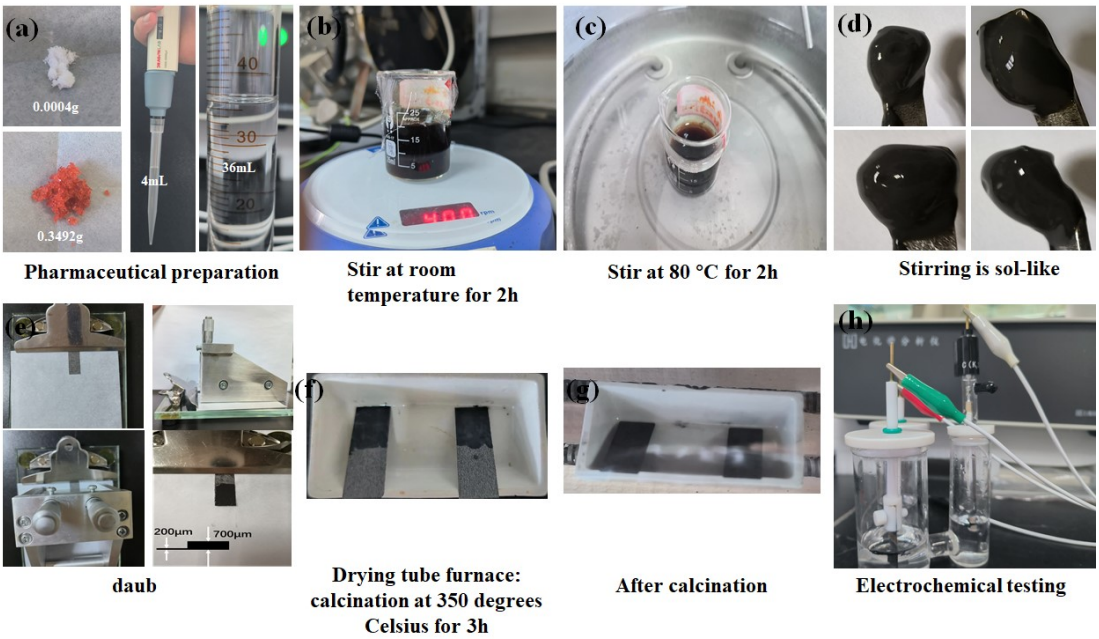

Fig. S1 Experimental details

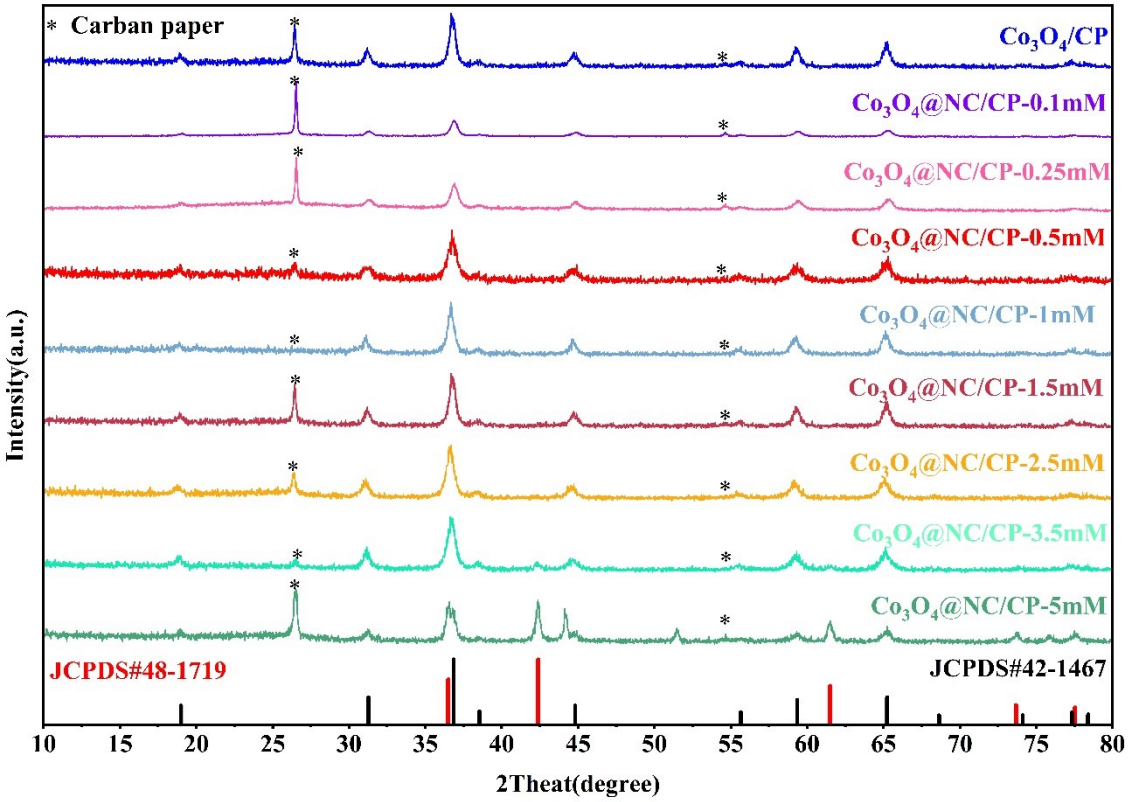

Fig. S2 XRD of Co_3O_4/CP, Co_3O_4@NC/CP-0.25mM, Co_3O_4@NC/CP-0.5mM, Co_3O_4@NC/CP-1mM, Co_3O_4@NC/CP-1.5mM, Co_3O_4@NC/CP-2.5mM, Co_3O_4@NC/CP-3.5mM, and Co_3O_4@NC/CP-5mM. * is the carbon paper, the black signals (JCPDS#42-1467) represent the spinel type of Co_3O_4 structure and the red signals (JCPDS#48-1719) represent the CoO structure.

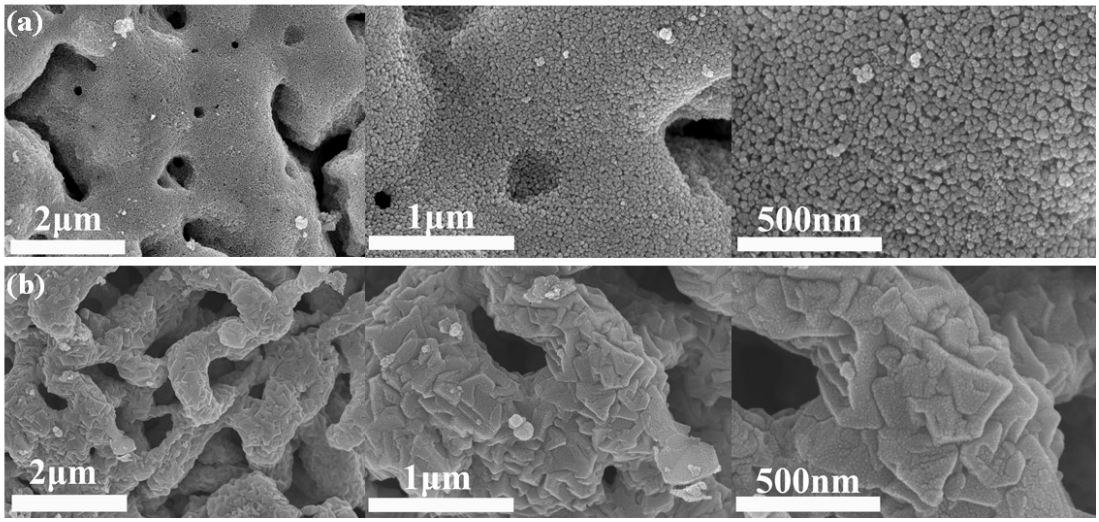

Fig. S3 (a) SEM of Co_3O_4. (b) SEM of Co_3O_4@NC-2.5mM.

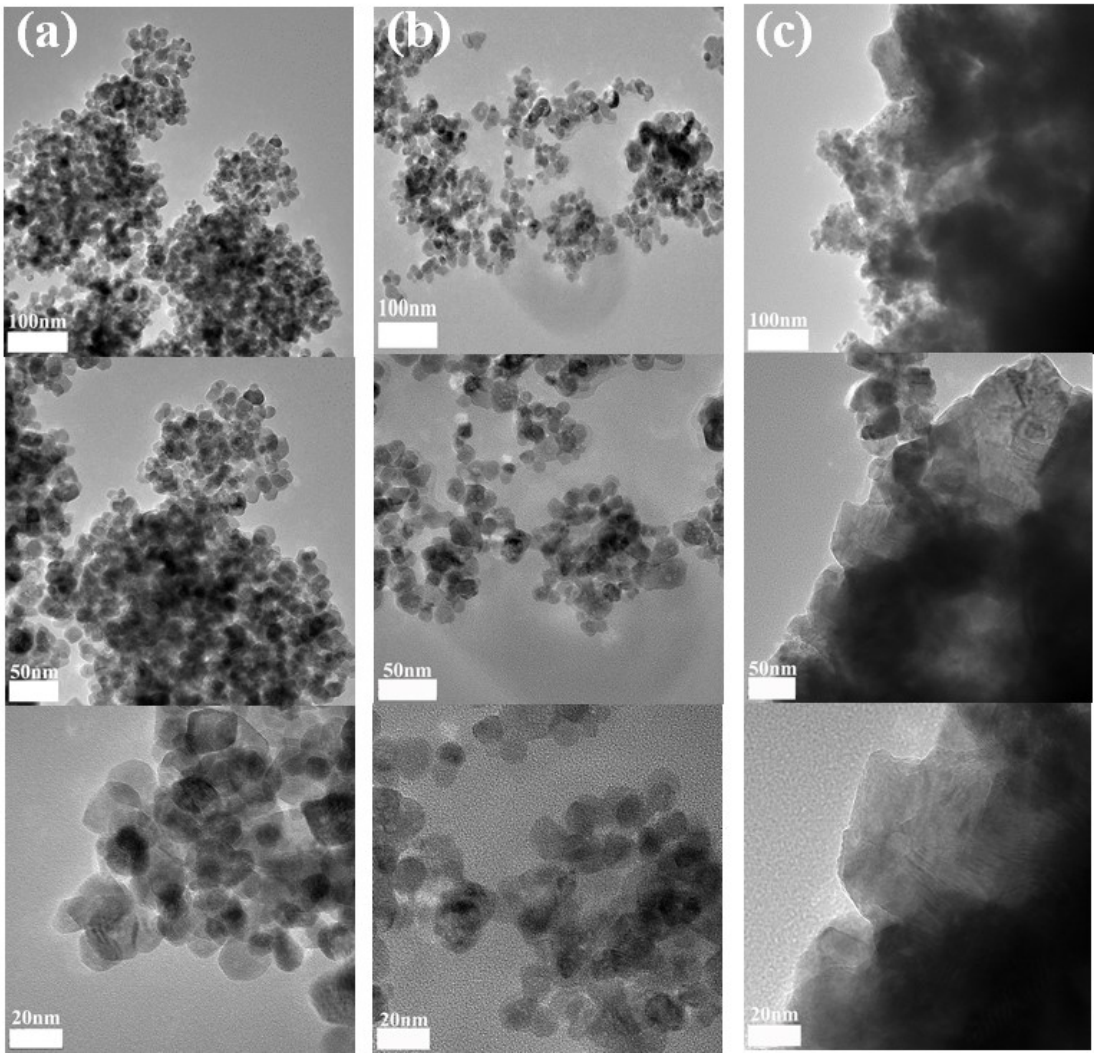

Fig. S4 (a), (b), and (c) are the TEM of Co_3O_4@NC-0.5mM, Co_3O_4, and Co_3O_4@NC-2.5mM, respectively.

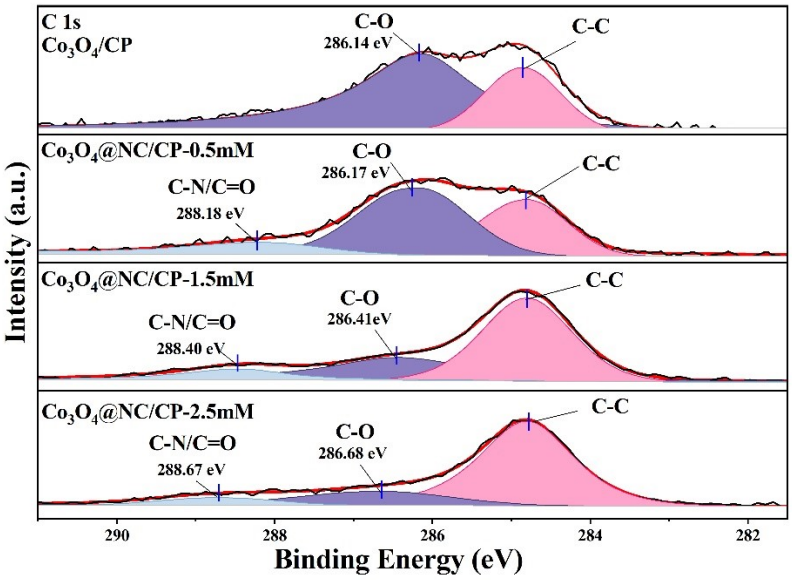

Fig. S5 C1s XPS spectra of Co_3O_4@NC-0.5mM, 1.5 and 2.5mM.

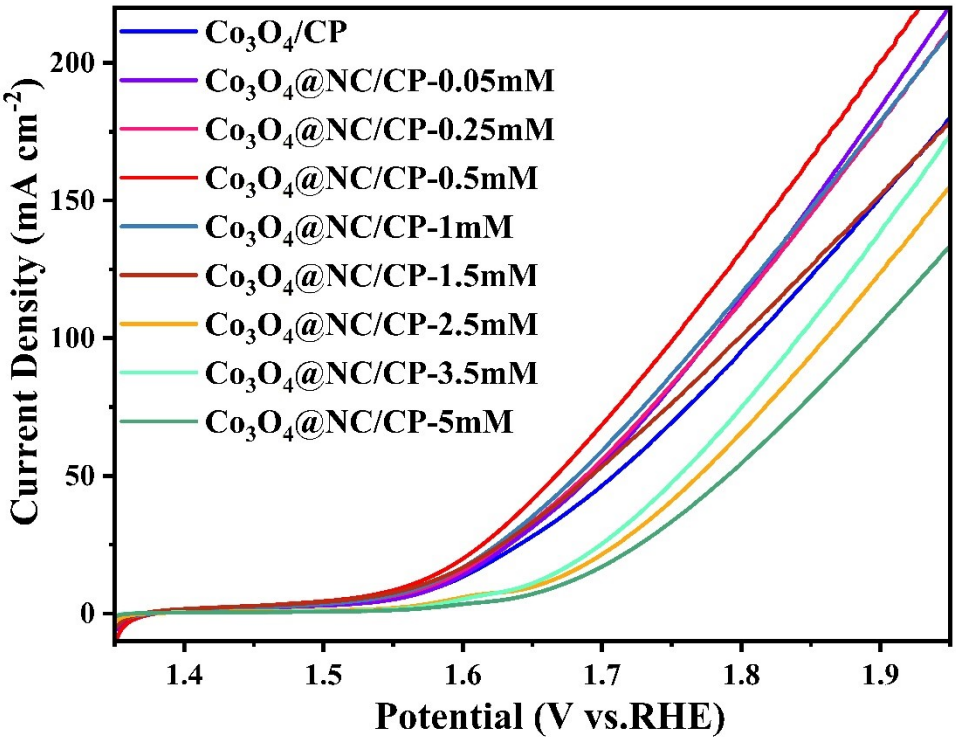

Fig. S6 LSV at different molar ratios for Co_3O_4/CP, Co_3O_4@NC/CP-0.1mM, Co_3O_4@NC/CP-0.25mM, Co_3O_4@NC/CP-0.5mM, Co_3O_4@NC/CP-1mM, Co_3O_4@NC/CP-1.5mM, Co_3O_4@NC/CP-2.5mM, Co_3O_4@NC/CP-3.5mM, and Co_3O_4@NC/CP-5mM.

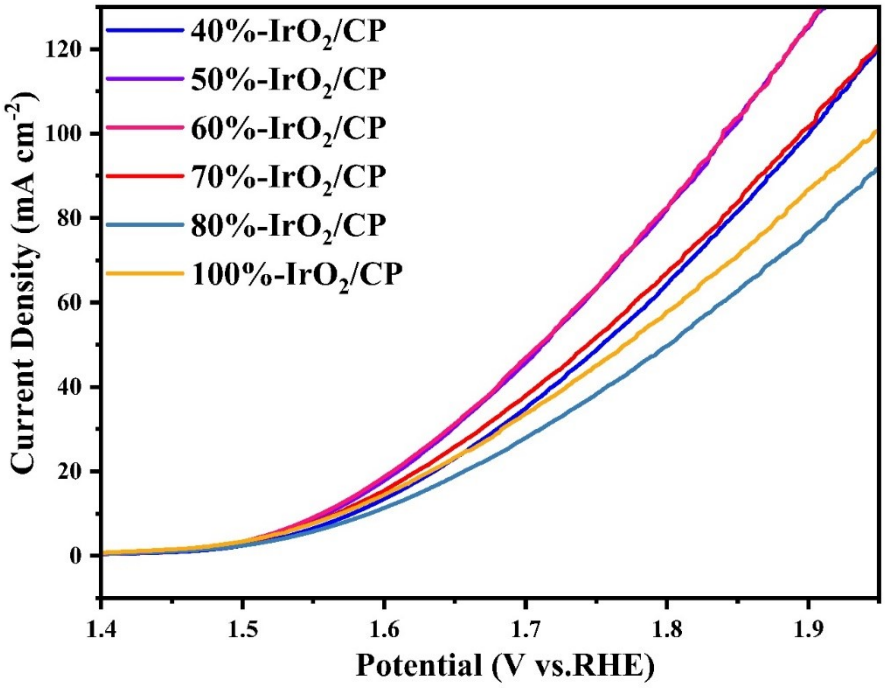

Fig. S7 LSV of different content of IrO_2

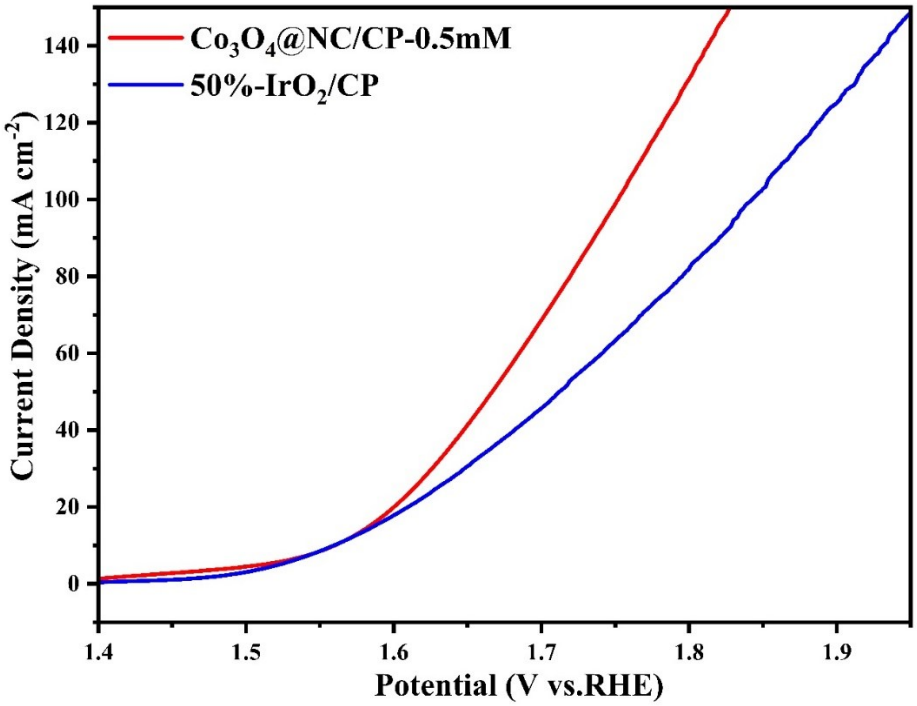

Fig. S8 Comparison of LSV for commercial IrO_2 (the best) and Co_3O_4@NC

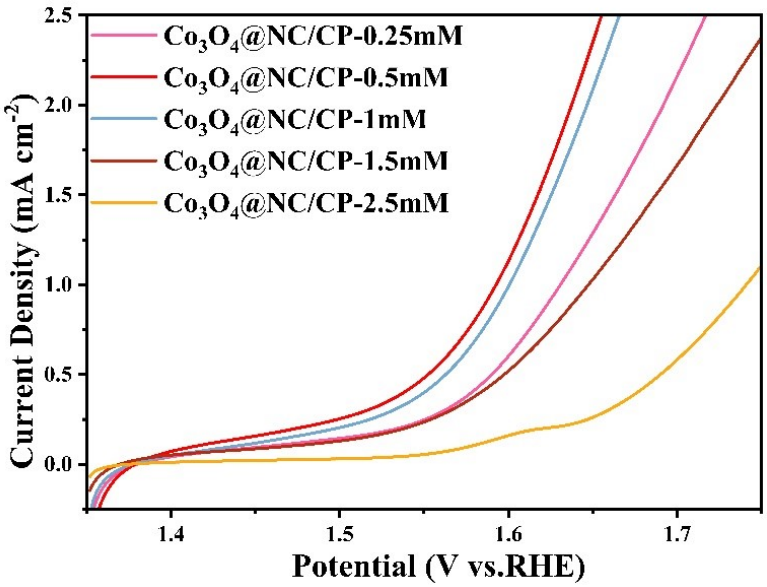

Fig. S9 LSV curves were normalized according to the Co_3O_4 ECSA

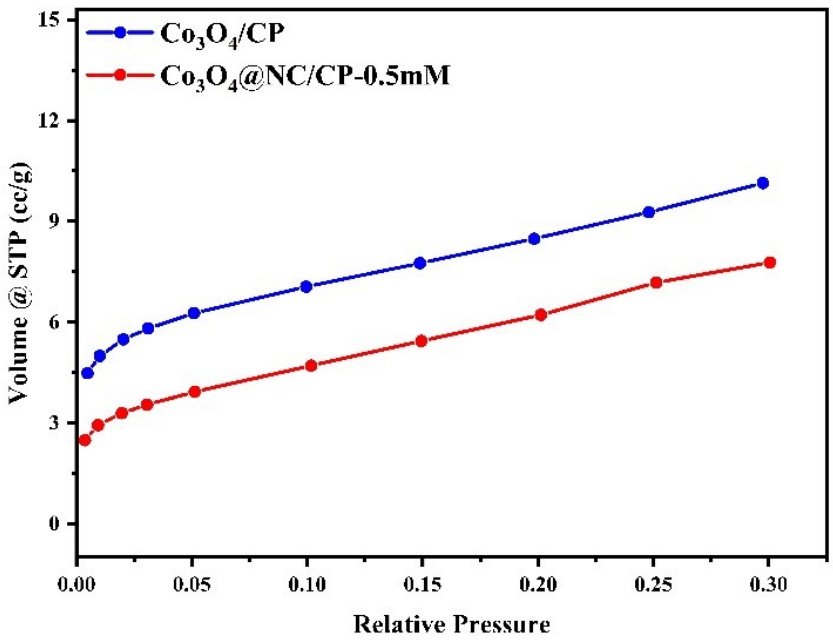

Fig. S10 Isothermal adsorption curves of Co_3O_4@NC/CP-0.5mM and Co_3O_4/CP

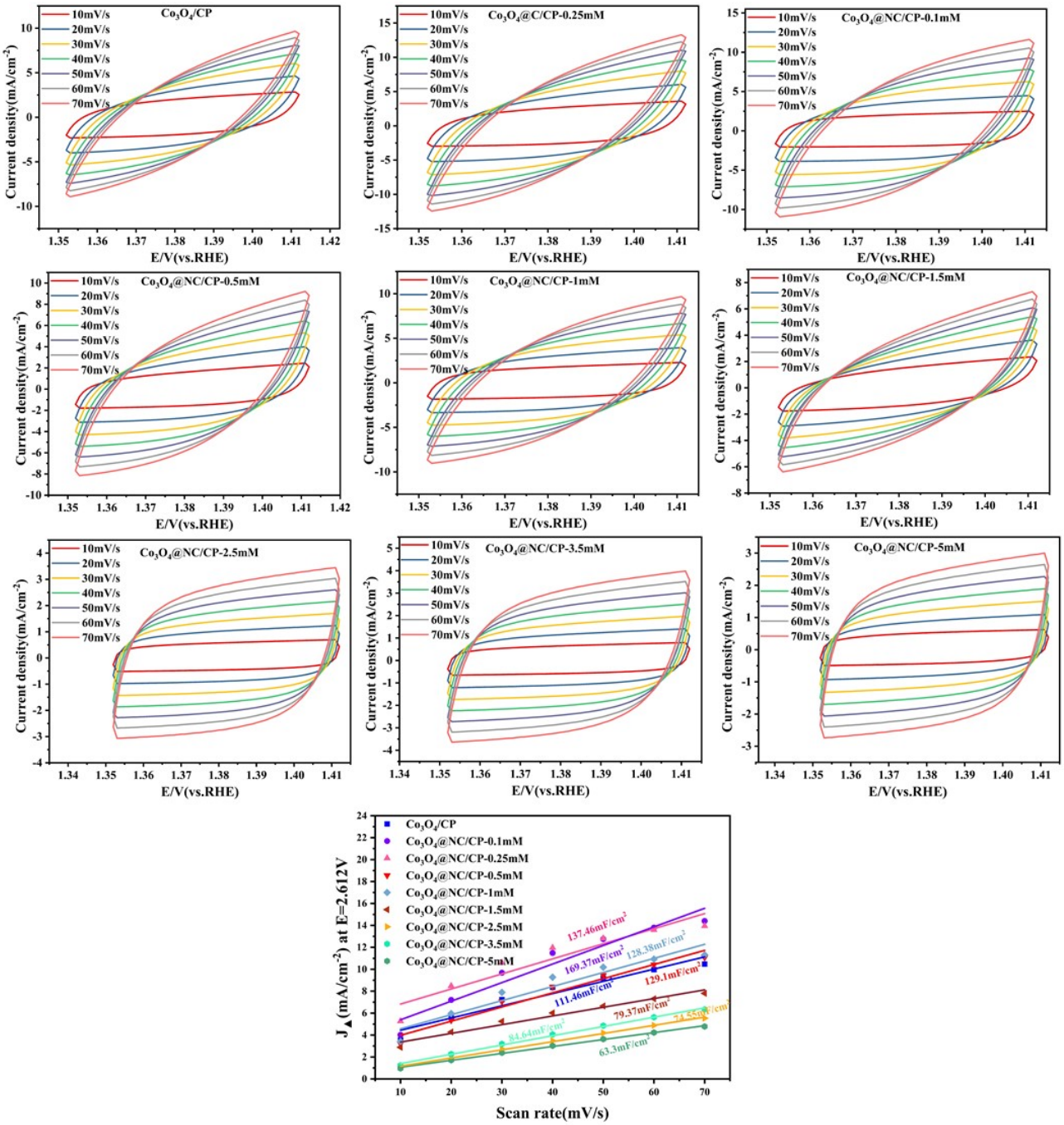

Fig. S11 Cyclic voltammograms (CV) and double-layer capacitor (C_{dl}) for Co_3O_4/CP, Co_3O_4@NC/CP-0.1mM, Co_3O_4@NC/CP-0.25mM, Co_3O_4@NC/CP-0.5mM, Co_3O_4@NC/CP-1mM, Co_3O_4@NC/CP-1.5mM, Co_3O_4@NC/CP-2.5mM, Co_3O_4@NC/CP-3.5mM, and Co_3O_4@NC/CP-5mM.

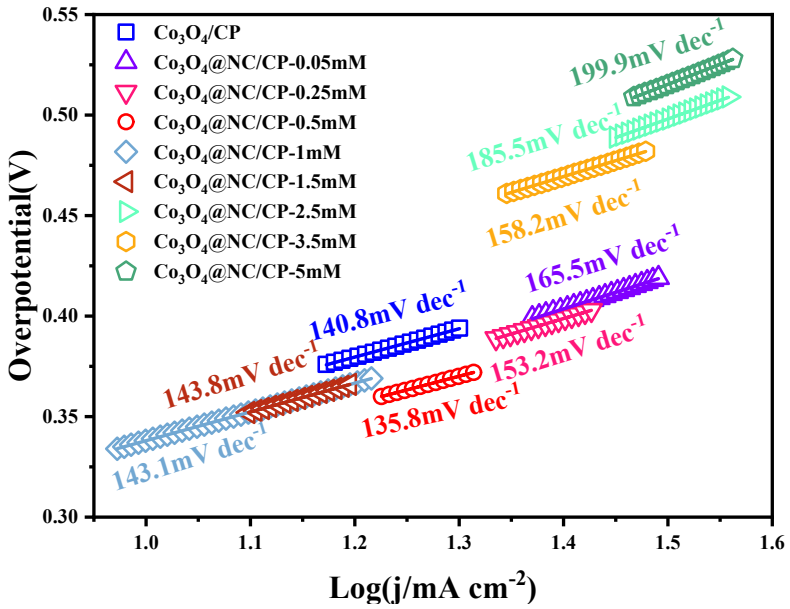

Fig. S12 Tafel slop of Co_3O_4/CP, Co_3O_4@NC/CP-0.05 5mM.

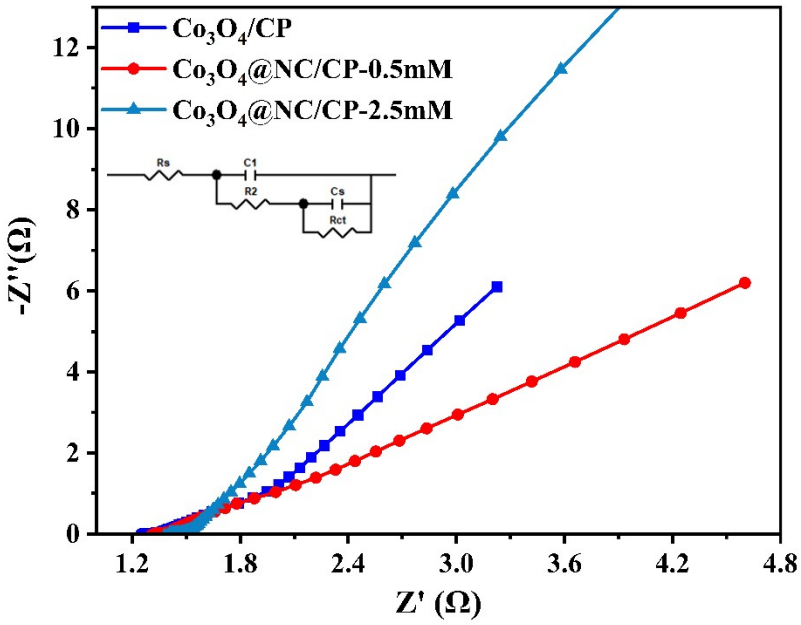

Fig. S13 Electrochemical impedance spectroscopy (EIS) for Co_3O_4/CP, Co_3O_4@NC/CP-0.5 and Co_3O_4@NC/CP-2.5mM.

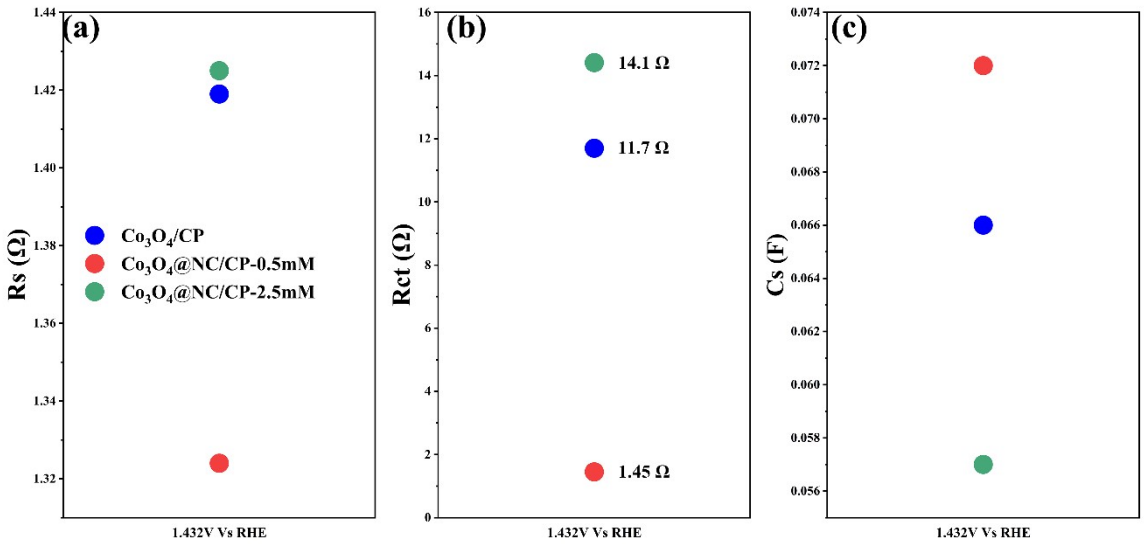

Fig. S14 Fitted parameters from the above EIS: (a) Series resistance, Rs, (b) Charge transfer resistance, Rct and (c) Surface capacitance, C_S.

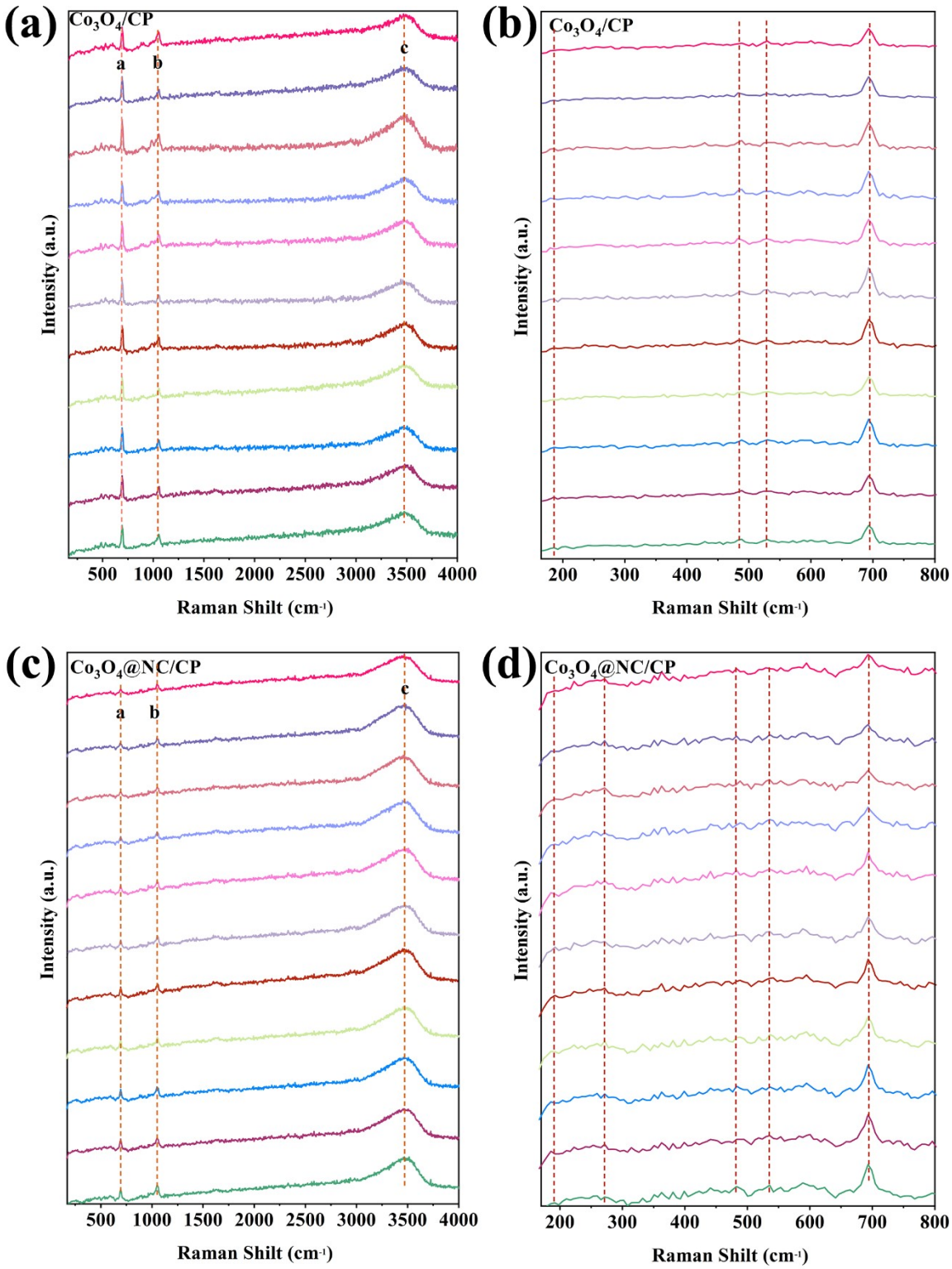

Fig. S15 Time-dependent in situ Raman spectra of as-prepared catalysts during OER process by an applied voltage (10mA cm^{-2} constant current, step size 30s. (a), (b) in situ Raman spectra of Co_3O_4/CP. (c), (d) in situ Raman spectra of Co_3O_4@NC/CP-0.5mM. peak a is [CoO_6] octahedra: ~690 cm^{-1}; peak b is SO_4^{2-}: ~1000 cm^{-1}; and peak c is OH: ~3500 cm^{-1}; [CoO_4] tetrahedra: ~196 cm^{-}

[1]; $Co(OH)_2$: ~290 cm^{-1}; Co-O bending and Co-O stretching in CoOOH: ~480 cm^{-1} and ~520 cm^{-1}, respectively.

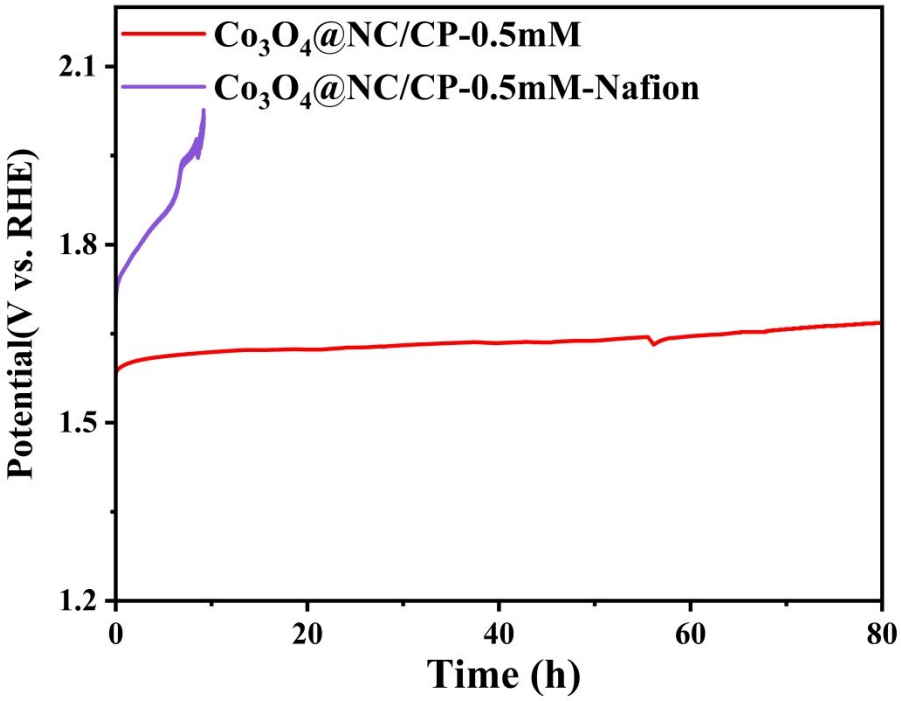

Fig. S16 The stability of in situ growth Co_3O_4@NC/CP-0.5mM and naphthol bonding Co_3O_4@NC-0.5mM.

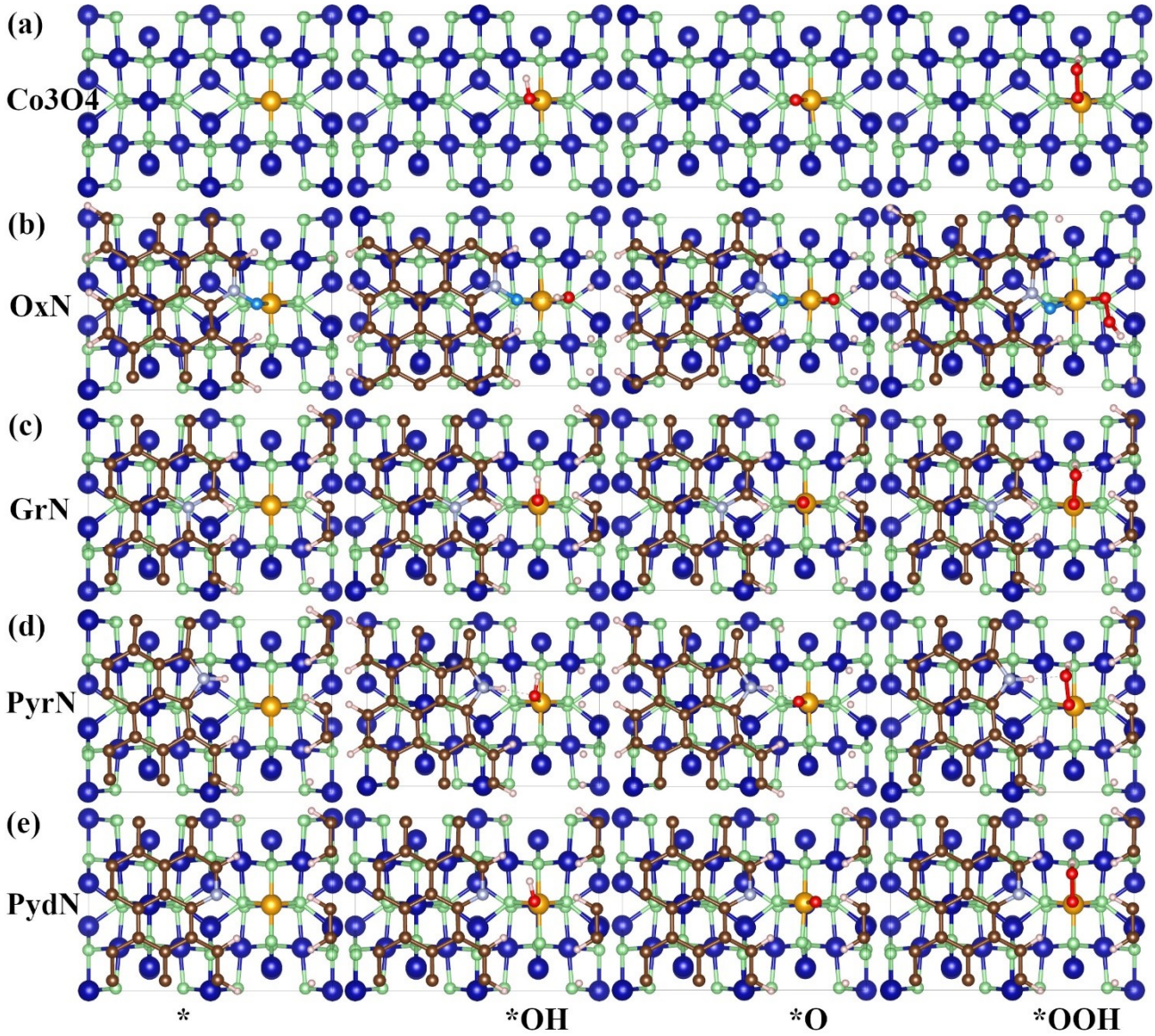

Fig. S17 Optimized configurations of intermediates for (a) pure Co_3O_4(110), (b) Oxidized N, (c) Graphitic N, (d) Pyrrolic N and (e) Pyridinic N carbonaceous components covered Co_3O_4. Orange: reactive cobalt site; blue: cobalt; lightgreen: oxygen of Co_3O_4; red: oxygen of intermediates; dodgerblue: oxygen of NO group; brown: carbon; pink: hydrogen; and lightblue: nitrogen.

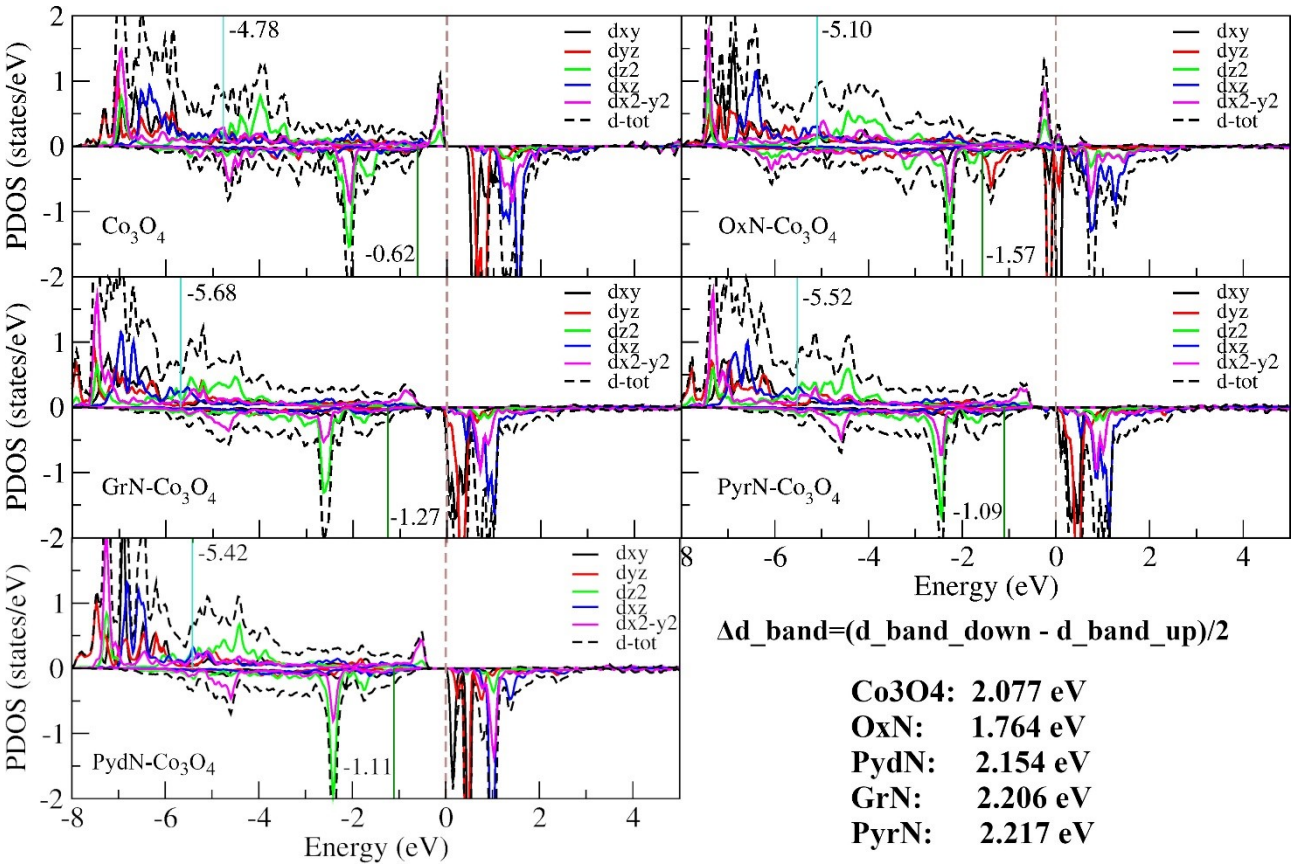

Fig. S18 Projected density of states (PDOS) of the active Co (orange site in Fig. S13) for (a) pure Co_3O_4(110), (b) Oxidized N, (c) Graphitic N, (d) Pyrrolic N and (e) Pyridinic N carbonaceous components covered Co_3O_4. The d_band of spin-up and spin-down are marked by turquoise and green vertical line, respectively. We defined the difference of d_band (Δd_band) between these two spin channels as: half of d_band(down) minus d_band(up).

Table S1 Calculated Gibbs energies of O_2, H_2, H_2O and OH. where G_{O2} are evaluated as $G_{O2} = 2 * (G_{H2O} - G_{H2}) + 4.92$

	E	TS	ZPE	G	G-reference[a]
O_2	/	/	/	-9.705	-9.717
H_2	-6.771	0.316	0.279	-6.808	-6.807
H_2O	-14.213	0.483	0.575	-14.121	-14.126

a. from ref [1]

Table S2 Performance parameters for different electrocatalysts for OER in strong acidic electrolytes.

Catalysts	j (mA cm^{-2})	η (mV)	Electrolyte
Co_3O_4@C/CP[2]	10	370	0.5 M H_2SO_4
Co_3O_4@C/GPO[3]	10	356	1 M H_2SO_4
Co_3O_4 /GC[4]	10	470	0.5 M H_2SO_4
Co_3O_4/FTO[5]	10	570	0.5 M H_2SO_4
Fe- Co_3O_4 @C/FTO [6]	10	396	0.5 M H_2SO_4
[Co-Fe-Pb]Ox[7]	10	560±10	0.5 M H_2SO_4
$Co_{0.05}Fe_{0.95}Oy$[8]	10	650	0.5 M H_2SO_4
Co_2TiO4[9]	10	513	0.5 M H_2SO_4
Ag-Co/FTO[10]	10	370	0.5 M H_2SO_4
Fe_2O_3[11]	10	650	0.5 M H_2SO_4
LaMn@NCo-ZIF [12]	10	353	0.1M$HClO_4$
Co_3O_4/CP (This work)	10	365	1 M H_2SO_4
Co_3O_4@NC/CP (This work)	10	330	1M H_2SO_4

Table S3 Bader charges (*e*) of carbonaceous component (CC) and the Co_3O_4 component. The positive value means electrons gained; and the negative one means losing electrons.

	C	O(C)[a]	N	H	sum(CC)	Co	O(Co_3O_4)[b]	sum(Co_3O_4)
Co_3O_4	/	/	/	/	/	-52.858	52.793	-0.0655 [c]
OxN	-0.720	0.589	0.584	-0.748	-0.295	-52.497	52.725	0.228
PydN	-1.040	/	1.203	-0.619	-0.456	-52.525	52.914	0.389
GrN	-1.012	/	1.193	-0.847	-0.666	-52.432	53.031	0.599
PyrN	-0.604	/	1.133	-1.082	-0.553	-52.508	52.993	0.485

a. Oxygen of carbonaceous component; b. oxygen of Co_3O_4 component; c. not equal to 0 because the symmetric model is nonstoichiometric and arises from the error of calculations. However, the relative charges are more meaningful.

References

1 Y. Zhou and N. López, *ACS Catal.*, 2020, **10**, 6254–6261.

2 X. Yang, H. Li, A.-Y. Lu, S. Min, Z. Idriss, M. N. Hedhili, K.-W. Huang, H. Idriss and L.-J. Li, *Nano Energy*, 2016, **25**, 42–50.

3 J. Yu, F. A. Garcés-Pineda, J. González-Cobos, M. Peña-Díaz, C. Rogero, S. Giménez, M. C. Spadaro, J. Arbiol, S. Barja and J. R. Galán-Mascarós, *Nat Commun*, 2022, **13**, 4341.

4 K.-L. Yan, J.-F. Qin, J.-H. Lin, B. Dong, J.-Q. Chi, Z.-Z. Liu, F.-N. Dai, Y.-M. Chai and C.-G. Liu, *J. Mater. Chem. A*, 2018, **6**, 5678–5686.

5 J. S. Mondschein, J. F. Callejas, C. G. Read, J. Y. C. Chen, C. F. Holder, C. K. Badding and R. E. Schaak, *Chem. Mater.*, 2017, **29**, 950–957.

6 D. Senthil Raja, P.-Y. Cheng, C.-C. Cheng, S.-Q. Chang, C.-L. Huang and S.-Y. Lu, *Applied Catalysis B: Environmental*, 2022, **303**, 120899.

7 D. Simondson, M. Chatti, S. A. Bonke, M. F. Tesch, R. Golnak, J. Xiao, D. A. Hoogeveen, P. Cherepanov, J. L. Gardiner, A. Tricoli, D. R. MacFarlane and A. N. Simonov, *Angewandte Chemie International Edition*, 8.

8 M. R. Cerón, M. Izquierdo, N. Alegret, J. A. Valdez, A. Rodríguez-Fortea, M. M. Olmstead, A. L. Balch, J. M. Poblet and L. Echegoyen, *Chem. Commun.*, 2016, **52**, 64–67.

9 S. Anantharaj, K. Karthick and S. Kundu, *Inorg. Chem.*, 2019, **58**, 8570–8576.

10 K.-L. Yan, J.-Q. Chi, J.-Y. Xie, B. Dong, Z.-Z. Liu, W.-K. Gao, J.-H. Lin, Y.-M. Chai and C.-G. Liu, *Renewable Energy*, 2018, **119**, 54–61.

11 W. L. Kwong, C. C. Lee, A. Shchukarev, E. Björn and J. Messinger, *Journal of Catalysis*, 2018, **365**, 29–35.

12 L. Chong, G. Gao, J. Wen, H. Li, H. Xu, Z. Green, J. D. Sugar, A. J. Kropf, W. Xu, X.-M. Lin, H. Xu, L.-W. Wang and D.-J. Liu, *Science*, 2023, **380**, 609–616.